

***In vivo* confocal imaging of epidermal cell migration and dermal changes post nonablative fractional resurfacing: study of the wound healing process with corroborated histopathologic evidence**

Oliver F. Stumpp
Vikramaditya P. Bedi
Danica Wyatt
Diana Lac

Solta Medical
25881 Industrial Boulevard
Hayward, California 94545

Zakia Rahman

Solta Medical
25881 Industrial Boulevard
Hayward, California 94545
and
Stanford University
School of Medicine
Stanford, California 94305

Kin F. Chan

Solta Medical
25881 Industrial Boulevard
Hayward, California 94545

Abstract. *In vivo* wound healing response post nonablative fractional laser treatment is evaluated. Seven healthy subjects receive treatments with a Fraxel *re:store*TM laser system on the forearm with pulse energies ranging from 10 to 70 mJ. The treatment sites are imaged at 1-h increments up to 40 h using confocal microscope z-stacks using 10- μ m-depth spacing. At least five individual microscopic treatment zones are imaged per subject, time point, and treatment energy. Images are analyzed for tissue structure and morphology to classify each lesion as healed or not healed, depending on epidermal re-epithelialization at each time point and treatment energy. Probit analysis is used to statistically determine the ED₅₀ and ED₈₄ probabilities for a positive dose response (healed lesion) as a function of treatment energy. Confocal observations reveal epidermal keratinocyte migration patterns confirmed with histological analysis using hematoxylin and eosin (HE) and lactate dehydrogenase (LDH) staining at 10 mJ at 0, 7, 16, and 24-h post-treatment. Results indicate that more time is required to conclude re-epithelialization with larger lesion sizes (all less than 500 μ m) corresponding to higher treatment energies. For the entire pulse energy range tested, epidermal re-epithelialization concludes between 10 to 22-h post-treatment for ED₅₀ and 13 to 28 h for ED₈₄. © 2009 Society of Photo-Optical Instrumentation Engineers. [DOI: 10.1117/1.3103316]

Keywords: *in vivo* confocal imaging; wound healing; z-stacks; epidermal re-epithelialization; fractional photothermolysis.

Paper 08387R received Oct. 29, 2008; revised manuscript received Jan. 16, 2009; accepted for publication Jan. 20, 2009; published online Apr. 23, 2009.

1 Introduction

Nonablative fractional resurfacing (NFR) treatment has become a widely accepted modality for the treatment of periorbital wrinkles, pigmented lesions, melasma, as well as acne and surgical scars. This technological revolution was first enabled through the introduction of the Fraxel® SR750 laser in April of 2004¹ and continues with the current Fraxel *re:store*TM laser system. NFR treatment is a safe and predictable procedure that offers many significant advantages over the historical bulk treatment approach.^{2,3} Most significantly, the ultrastructure of the stratum corneum remains intact after the treatment due to the utilization of selective photothermolysis.¹ Patients can apply make-up and return to their daily activities on the same or following day with little or no down time.^{4,5}

Rather than relying on aggressive bulk ablative and nonablative treatment regimes, NFR treatment places well defined microscopic treatment zones (MTZs) of coagulated and ther-

mally denatured columns into tissue. Within each isolated MTZ, there is full thickness coagulation and collagen denaturation. However, with the fractional approach, the zone of injury is concentrated within the MTZ, and therefore the surrounding viable tissue acts as a reservoir of stem cells, growth factors, and inflammatory cells that quickly respond to and facilitate rapid re-epithelialization and thus rapid wound healing.^{1,6}

Skin resurfacing takes place biologically as nonviable keratinocytes are rapidly replaced by new ones, pushing necrosed tissue upward to eventually form microscopic epidermal necrotic debris (MEND) on the skin surface.⁷ As the wound healing response extends beyond the boundaries of each MTZ, the net effect is an accelerated turn-over process of the entire epidermal tissue. Epidermal re-epithelialization within MTZs takes place within approximately 15 to 24 h, while biological skin resurfacing is initiated, as indicated by slight bronzing (MEND) and scaling, followed by desquamation or exfoliation over the following 3 to 5 days.⁷ The risks of a delayed epidermal re-epithelialization process beyond the first

Address all correspondence to: Oliver F. Stumpp, Solta Medical, 25881 Industrial Blvd., Hayward, 94545. Tel. 650-605 2308; Fax. 650-605 2808; E-mail: laserscience@gmail.com.

24 to 48 h could lead to adverse clinical side effects, which alters the purpose and benefits of fractional treatment.⁸

In the recent past, a plethora of alternative laser devices have flooded the market claiming to provide fractional treatment with the same rapid wound healing profile. However, because stamping and computer pattern generator (CPG) scanners are cumbersome and slow in laying down individual treatment spots, these devices either are limited to low-coverage treatments, take significantly longer time to produce high-coverage treatments, or tend to operate with larger optical spot sizes to increase the treatment coverage, which in turn can have adverse clinical effects.

The aims of this study were to investigate if and how the lesion size, as a result of treatment energy, affects the wound healing process, and to determine the time point of complete epidermal re-epithelialization as a function of treatment energy, including keratinocyte migration patterns during wound healing.

2 Materials and Methods

Seven healthy subjects of Fitzpatrick skin types 2 through 4 gave their informed, written consent under an institutional review board (IRB) approved study protocol and in accordance with the declaration of Helsinki protocols to receive treatment on their forearms with a Fraxel *re:store*TM laser system. Pulse energies were varied from 10 to 70 mJ. The local cellular wound healing response was documented as a function of time using a VivaScope 1500 confocal reflectance microscope (Lucid, Incorporated, Rochester, New York) operating at 830 nm. This noninvasive imaging instrument allowed visual recording of tissue structures to a depth of approximately 200 μm below the skin surface, which captured the complete epidermis and the superficial papillary dermis. The 3-D nature of individual MTZs was captured by taking sets of confocal images at each location of interest, which were automatically captured sequentially with increasing depth. These so-called z-stacks were acquired at 10- μm -depth increments in 1-h time intervals starting immediately up to 35-h post-treatment.

Time-resolved imaging of lesions with confocal z-stacks allowed detailed analysis of epidermal wound healing and keratinocyte migration into the area of coagulated tissue within each microscopic treatment zone (MTZ). Statistically relevant data was obtained by analyzing multiple MTZs within the field of view of the confocal microscope. At each point in time, the status of epidermal re-epithelialization was decided, depending on the cellular morphologic structure at the dermal-epidermal junction (DEJ) observed with the confocal image. Since wound healing is a continuous process, a meaningful statistical analysis was based on a binary decision. At each time point it was decided whether the DEJ was completely re-epithelialized or not. There were several characteristic features that allowed distinguishing between treated and untreated or healed tissue, the last of which predominantly was comprised of new, viable epidermal keratinocytes.

The state of tissue healing was categorized as either healed or not healed, the former of which was determined by the following criteria.

- The tissue must be free of disruption, and appear contiguous throughout, with no open cracks and dark voids.

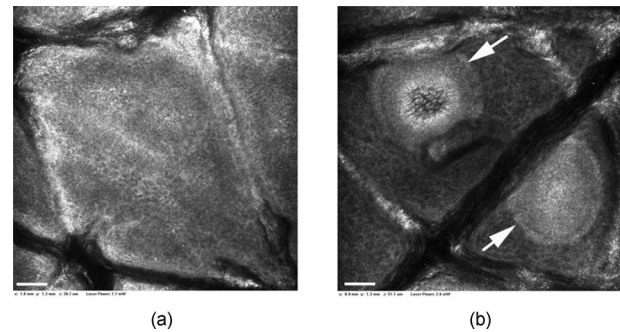


Fig. 1 Confocal images of (a) untreated skin showing epidermis and viable keratinocytes, and (b) Fraxel *re:store*TM laser treated skin 3-h post-20-m treatment (arrows indicate the lesions). Scales represent 50 μm .

- The epidermis must display visibly viable cellular features, similar to untreated tissue.
- There must be a smooth transition from the epidermis to the dermis and an intact rete-ridge pattern

Each MTZ was compared against all of these criteria at each point in time. For a thorough analysis, it was imperative to consider the entire z-stacks taken for all lesions. Once all of the criteria had been met, an MTZ was considered healed.

Binary results obtained as a function of treatment energy and time were fit into a dose response format and were then statistically analyzed using Probit analysis.^{9,10} This type of analysis permits calculating discrete values of probability, also referred to as ED_x values, where x denotes the probability for a positive dose response, thus a lesion being classified as healed. These calculations were based on the assumption of a 95% confidence level and 0.1 heterogeneity test. In this study, 50 and 84% probabilities were chosen to determine ED_{50} and ED_{84} values.

The confocal analysis was also complemented with histological analysis. Subjects were biopsied immediately, 7, 16, and 24 h following treatment at pulse energy 10 mJ. The biopsy was cut into two halves. One half of the biopsy was fixed with neutral buffered formalin phosphate (VWR International, West Chester, Pennsylvania) at room temperature and embedded in paraffin, while the other half was frozen embedded in Optimal Temperature Cutting Fluid (VWR International, West Chester, Pennsylvania). The paraffin embedded blocks were cut into 5- μm -thick sections and stained with hematoxylin and eosin (HE), while the frozen embedded samples were cut into 20- μm -thick sections and were stained with nitro blue tetrazolium chloride (NBTC) (Sigma-Aldrich Corporation, Saint Louis, Missouri) for lactate dehydrogenase (LDH) activity. Lesions were imaged and recorded using a Leica[®] DM LM/P microscope and a DFC320 digital camera (Leica Microsystems, Cambridge, United Kingdom).

3 Results

The time-resolved wound healing response post-NFR treatment was studied using 3-D so-called z-stacks of confocal images of the individual MTZs. Figure 1 illustrates the difference between untreated epidermal tissue and treated tissue.

The normal or untreated epidermis features keratinocytes that appeared granular and in a honeycomb-like arrangement,

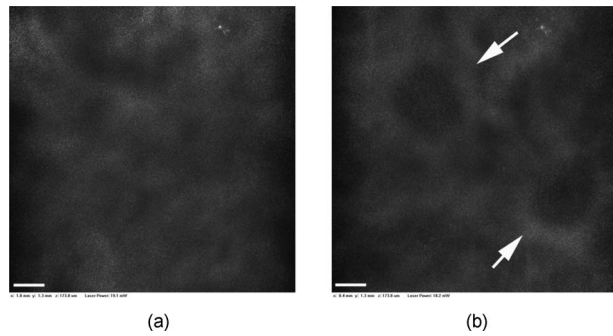


Fig. 2 Confocal appearance of untreated dermal tissue in (a) and confocal image of treated dermis (b) corresponding to the same site as epidermally shown in Fig. 1(b). Arrows are pointing to the individual lesions. Scales represent 50 μm .

with criss-crossing dark and wide bands of dermatoglyphs, indicating deeper skin crevices outside of the immediate image plane. Within an area receiving NFR treatment [Fig. 1(b)], MTZs could easily be identified with some lesions showing slight epidermal disruption (upper left) and coagulated epidermis without disruption, both resulting from laser treatment. The boundary between native and coagulated tissue is easily demarcated based on changes in back-reflected light and tissue morphological structure.

Although the useful imaging depth is limited to approximately 200 μm , confocal imaging of the superficial or papillary dermis was possible. Figure 2 shows images of the papillary dermis corresponding to the same location as epidermally shown in Figs. 1(a) and 1(b).

In the dermis, the coagulated dermal tissue within individual MTZs is easily identified by the dark circular areas surrounded by diffusely fibrillar structures that scatter light back.

Figure 3 illustrates an example of an epidermally completely healed MTZ 21-h post-40-mJ NFR treatment. The figure consists of nine representative images obtained from a confocal z-stack data cube, which show viable keratinocytes and a gradual, smooth transition across the dermal-epidermal junction (DEJ) separating the epidermis and the dermis. The dermal component of the MTZ compares to Fig. 2(b) and appeared unaltered from the coagulated state.

Image analysis was performed on all z-stacks at different treatment energies and time points. Based on the criteria outlined in the methods section, a lesion was classified as either healed or unhealed. This type of binary statistical data was analyzed using Probit analysis to yield probability and dose-response graphs for all treatment energies. As an example, Fig. 4 shows the probability and dose response for the 40-mJ treatment.

Furthermore, Probit analysis permits calculating probability values for a positive response at a given dose (time) for each treatment energy. Based on ED_{50} and ED_{84} values for a positive dose response at each treatment energy, the required time was determined and collectively plotted in Fig. 5 as a function of treatment energy. The upper and lower time limits at each treatment energy result from the assumed 95% confidence level.

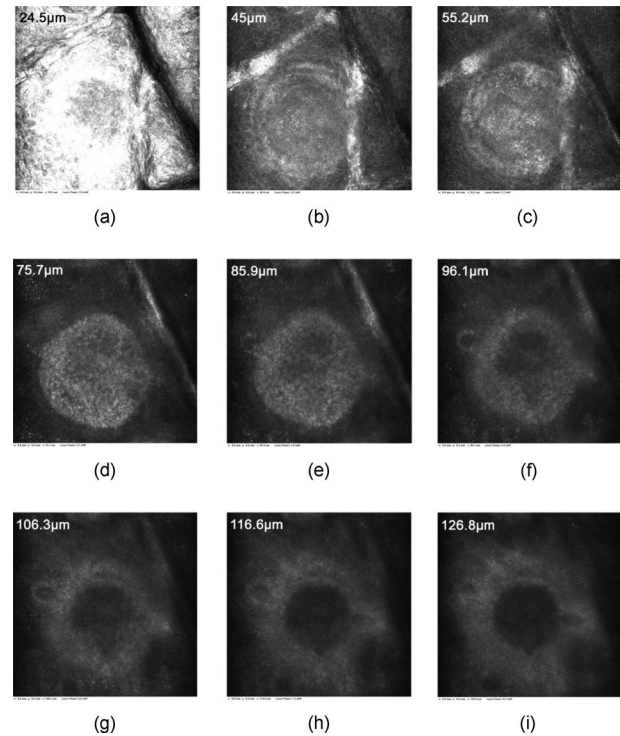


Fig. 3 Confocal z-stack of a 40-mJ MTZ 21-h post-treatment showing epidermal re-epithelialization and the remaining dermal coagulation.

Similarly, epidermal healing can be indirectly observed using white light photography and shows the formation of microscopic epidermal necrotic debris (MEND) over time. The onset and darkness of MEND depends on treatment energy and the amount of epidermal pigment (skin type). Due to the microscopic spot size, MENDs are only visible under magnification. Figure 6 shows magnified white light images of skin type 2 and one skin type 5 following treatment.

Epidermal disruption following NFR treatment such as shown in Fig. 1(b) was used as a uniquely identifying feature by which similar lesions could be recognized and tracked over the time course of epidermal healing. Being able to identify specific lesions and to perform time-resolved analyses proved useful beyond the mere statistical analysis of epidermal wound healing of like-lesions treated with the same laser parameter. The unique features of individual lesions served as landmarks that allowed tracking of epidermal keratinocyte migration and provided solid proof of epidermal cell turnover, DEJ closure, and ultimately re-epithelialization.

One example is shown in Fig. 7 where one MTZ with a characteristic pattern of epidermal disruption following a 40-mJ treatment is shown at a comparable imaging depth at different time points.

The lesion is easy to identify at the different time points, and comparison of the unique epidermal pattern of disruption over time reveals slow closure of the disrupted DEJ (dark gaps). At 3- and 7-h post-treatment migrating keratinocytes are visible as they slowly occupy the void spaces in the process of epidermal re-epithelialization.

Interested in validating and confirming our confocal observations, we used histological analysis at selected time points to analyze how fractionally treated tissue responds during

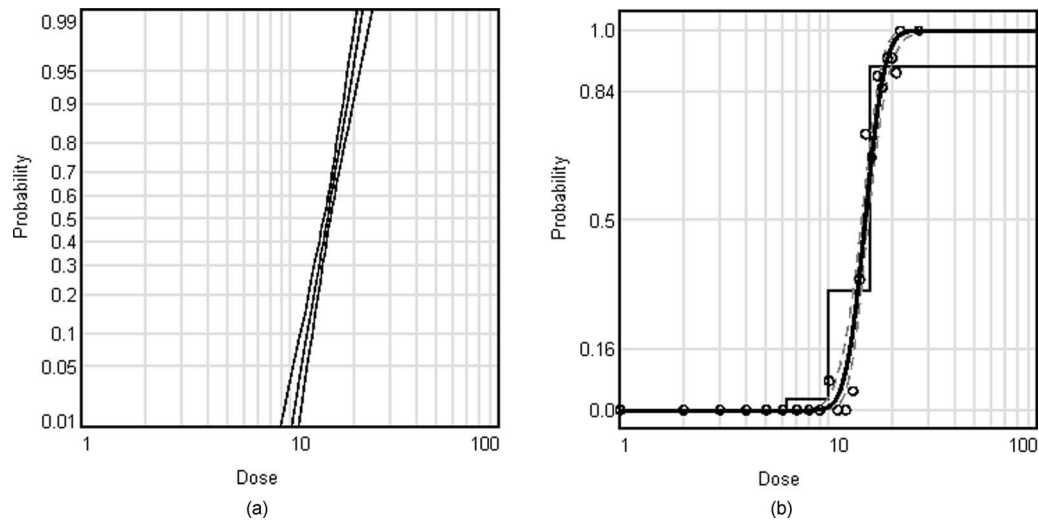


Fig. 4 Probability and dose-response curve for 40-mJ treatment energy. (a) shows the probability for a positive dose response and the fiducial limits based on a 95% confidence interval. (b) represents a Probit fit to the measured data (circles) at each time point (dose).

wound healing. Figure 8 shows HE-stained tissue sections at different time points following a 10-mJ treatment.

To better distinguish between treated, nonviable tissue and newly forming viable tissue, we extended our histological analysis to include LDH staining. Figure 9 shows micrographs of LDH-stained biopsies following a 10-mJ treatment. Biopsies were collected immediately following treatment and at 7, 16, and 24-h post-treatment corresponding to the HE sections shown in Fig. 8.

Figure 10 shows interesting modes of epidermal keratinocyte migration. Instead of migrating along the DEJ, these micrographs show viable suprabasal keratinocytes migrating across the MTZ diameter far above the DEJ. Interesting also was the observation of keratinocytes migrating just below the stratum corneum, as shown in Figs. 9(b) and 10(b).

Although the epidermal healing process concluded between 13 (10 mJ) to 23-h (60 mJ) post-treatment, there was no observable change in the coagulated dermis. However, we continued confocal follow-up observations and noticed dermal changes at around 40-h post-treatment. Most notably, there was no light scattered back from coagulated dermis, and as a result, the columns of coagulated collagen were void of structural features [Figs. 2(b) and 3]. Yet at 40 h and beyond, there was structural detail visible within the coagulated collagen. These were viable structures, most likely a result of backscattered light originated from fibroblasts and inflammatory cells. Figure 11 shows examples of dermal confocal views of MTZs 40-h post-treatment.

4 Discussion

The aim of this study was to investigate the tissue response post fractional photothermolysis induced by NFR treatment. Of particular interest were the average time required for epidermal re-epithelialization as a function of treatment energy and the migration pattern of keratinocytes during wound healing. The Fraxel *re:store*TM laser used in this study changes optical spot size as a function of treatment energy. The optical adjustment is optimized for maximum depth of coagulation

for a given treatment energy. At the same time, the system parameters ensure fractionally complete epidermal coagulation throughout the available range of treatment energies.

As expected, at all treatment energy settings, complete epidermal and dermal coagulation was achieved within the confines of the lesions, and the coagulated lesion diameter increased with higher treatment energy. For the entire treatment energy range, coagulated lesion diameters were less than 500 μm in diameter as determined by histological analysis.¹¹

Current literature suggests the utility of *in vivo* confocal microscopy to visualize skin wound healing.¹² The benefits are apparent, as this method eliminates the necessity for invasive techniques like biopsies. More so, obtaining biopsies is an inherently destructive process and does not permit continued monitoring of the natural wound healing process.^{13,14} As a result, it is impossible to follow a particular site of interest

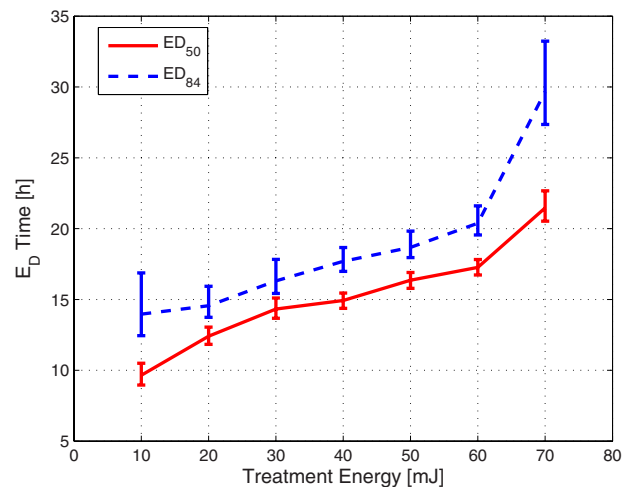


Fig. 5 Time points ED_x for 50 and 84% probability of a positive response, i.e., epidermally healed MTZ as a function of Fraxel *re:store*TM laser treatment pulse energy. Error bars result from the fiducial limits resulting from the assumed confidence interval.

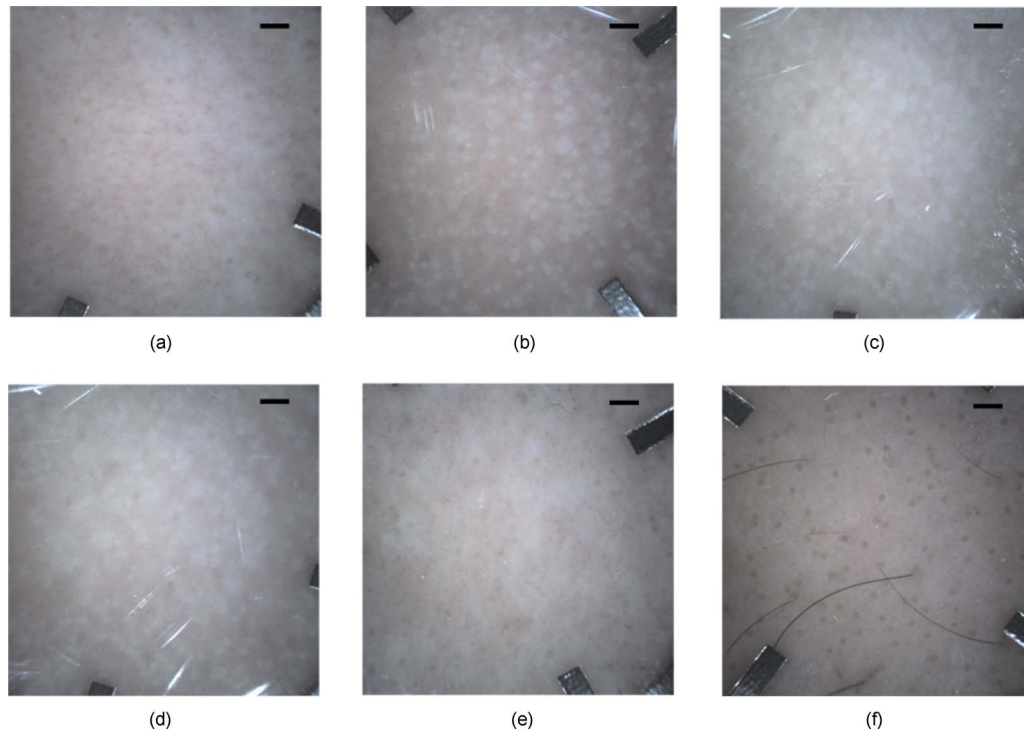


Fig. 6 Magnified white light images from one skin type 2 subject taken at different time points post-40-mJ NFR treatment: (a) immediately post-treatment, (b) 3 h, (c) 6 h, (d) 12 h, (e) 27 h, and a skin type 5 subject at (f) 14-h post-40-mJ NFR treatment. Scale bars represent 1 mm.

throughout the natural wound healing and remodeling phase unless a noninvasive optical imaging modality is employed. Using a confocal microscope, we were able to study and analyze epidermal wound healing, and in particular, re-epithelialization in great detail. We were fortunate to have had the chance to obtain numerous *in vivo* punch biopsies, which further helped validate the confocal findings using histology. The data presented confirmed our initial hypothesis that there is a distinct relationship between the diameter of epidermal coagulation, epidermal disruption, and the time required to complete epidermal re-epithelialization.

It was easy to distinguish between coagulated and native tissue using confocal imaging due to the differences in structural features. Morphologically, individual MTZs were characterized by a loss of cellular features in the epidermis. The coagulated tissue appeared mostly amorphous and revealed

little structural detail at best. Also, there was more backscattered light yielding increased image brightness compared to native tissue. The mechanical integrity of coagulated tissue was also visibly compromised. Minimal tissue disruption was manifested in confocal reflectance images as dark voids and cracks in the tissue. These areas with minimal disruption were filled with interstitial fluid, from which very little light was reflected back, as shown in Fig. 1. In contrast, the native epidermis resembled a granular, honeycomb-like structure rich in structural detail comprised of individual keratinocytes, cell membranes, and cellular nuclei.

Vastly different optical tissue properties in the dermis also yielded a characteristic imprint that permitted us to easily identify the location of the MTZs. Although there may have been less light available in the dermis due to a slight increase in scattering in coagulated epidermis, the absence of any de-

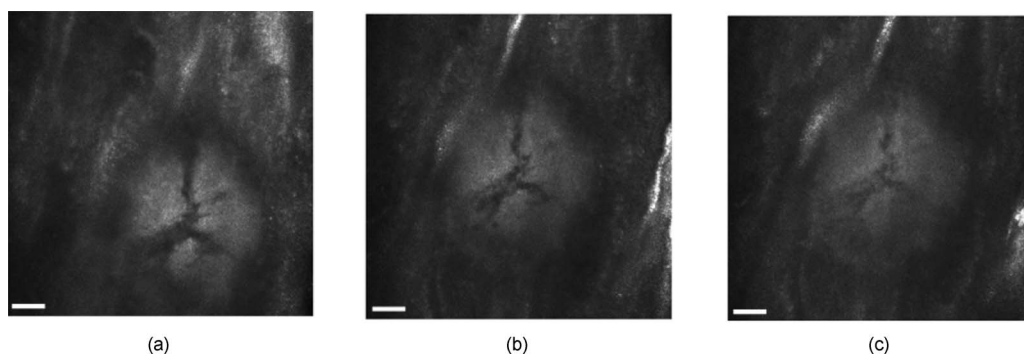


Fig. 7 A 40-mJ MTZ with characteristic pattern of epidermal disruption. Lesion imaged at approximately the same imaging depth (a) immediately, (b) 3 h, and (c) 7-h post-treatment. Scale bars represent 50 μm .

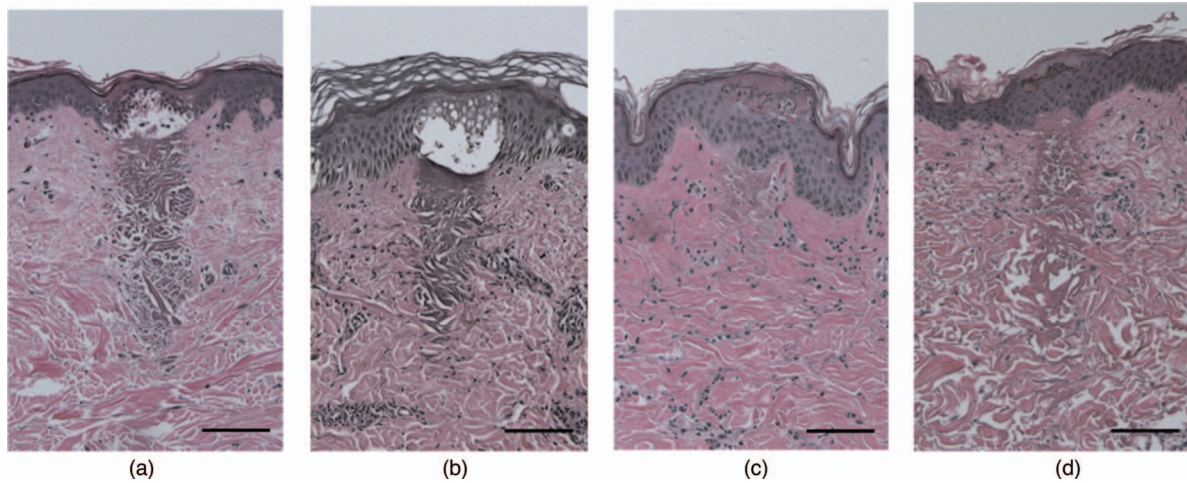


Fig. 8 HE-stained tissue sections from 10-m) treatment showing various epidermal wound healing phases. Images were taken at 10 \times ; scale indicates 100 μ m. Image time points are (a) immediately post-treatment, (b) 7 h, (c) 16 h, and (d) 24-h post-treatment.

tail in coagulated dermis was a clear indication of complete loss of birefringence and strong forward scattering (Fig. 2). In fact, a mere “shadowing” effect of superficially coagulated tissue could be ruled out, as these characteristic dark voids were also present long after the epidermal re-epithelialization process had concluded (Fig. 3). As such, the substantially brighter halo surrounding the coagulated column of dermal tissue was evidence of the ability to deliver photons deeper into tissue through these coagulated waveguides in comparison to untreated tissue.

As outlined in the methods in Sec. 2, the binary decision whether an MTZ was considered epidermally healed depended on a number of criteria, all of which had to be met simultaneously. The comparison of native and coagulated epidermal tissue (Fig. 1) gave rise to the first criterion that there must be visibly viable keratinocytes present in the previously coagulated tissue. Although MTZs could be identified by the

formation of MENDs near the skin surface, the characteristic features of the underlying dermal components provided ultimate proof and guidance in locating MTZs once re-epithelialization was complete or nearly complete. At the same time, as the DEJ was populated again by viable keratinocytes, epidermal disruption was repaired and no longer visible, i.e., tissue appeared contiguous. Repair of the DEJ also re-established the natural rete-ridge structure. This led to a confocally smooth, rather than abrupt, transition from epidermal to dermal features, as was observed in untreated control tissue. Only if all of these criteria were met was a lesion considered healed and counted as a positive response in the Probit analysis (Fig. 3).

The development of epidermal MENDs observed under white light imaging is shown in Fig. 6. While the optical spot size utilized during treatment is less than 500 μ m, and thus

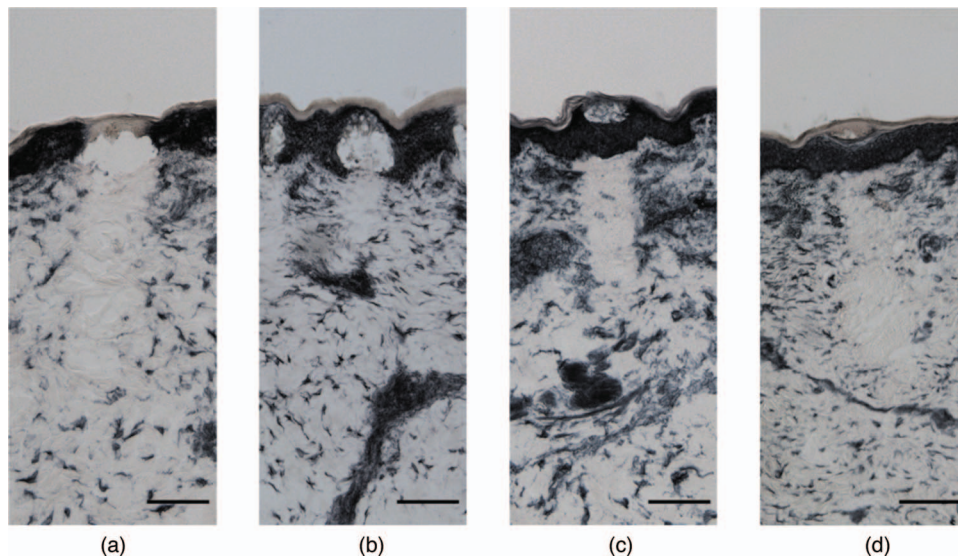


Fig. 9 LDH-stained tissue sections from 10-m) treatment throughout epidermal wound healing phase (a) immediately post-treatment, (b) 7 h, (c) 16 h, and (d) 24-h post-treatment. Images were taken at 10 \times ; scales indicate 100 μ m.

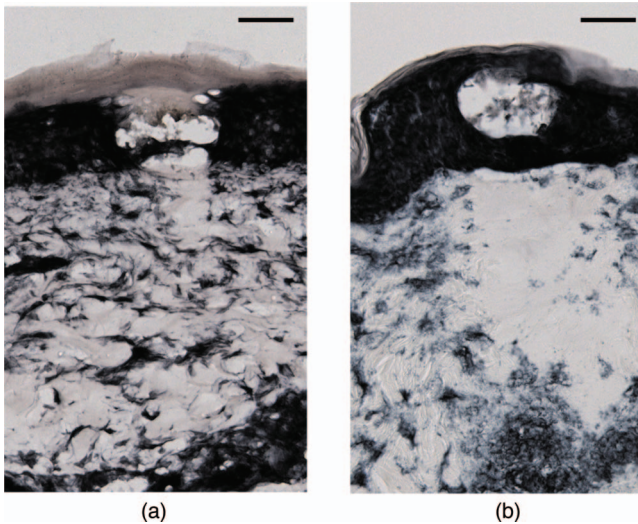


Fig. 10 LDH-stained tissue sections at (a) 7-h post-treatment and (b) at 16-h post-treatment showing evidence of suprabasal keratinocytes leapfrogging over the DEJ as opposed to migration of basal keratinocytes along the DEJ. Images are taken at 20 \times . Scales indicate 50 μ m.

small enough such that individual MTZs and later-forming MENDs are only visible to the unaided eye by very close or magnified inspection, the sequence of images presented in Fig. 6 documents the progression of MEND formation during the epidermal wound healing process. Initially, the microscopically coagulated epidermal tissue simply appeared slightly blanched and tended to darken over time. This step was also highly dependent on the skin type and the amount of pigment being resurfaced.⁶

We hypothesized that the cross sectional area of thermal and mechanical damage at the DEJ governs the time for the DEJ to recover and to facilitate epidermal re-epithelialization. The biochemical and biological processes involved in wound healing are derived from a cascade of events controlled and initiated by an inflammatory response. Also, often the topic of debate was how the DEJ is repaired and repopulated. It is thought that neighboring, viable basal keratinocytes eventually migrate along the DEJ into the damaged zone to form at least a monolayer of dividing basal keratinocytes to repair the epidermal damage from the ground up.^{15,16} The release of cytokines and the expression of heat shock protein are the harbingers of tissue remodeling. These early inflammatory responses result in a rearrangement of integrin receptors of viable keratinocytes neighboring the site of damage.^{17,18} These otherwise stationary cells first have to disconnect from their hemidesmosome anchoring points and express new integrins.^{15,19} Delocalized collagen receptors permit keratinocytes closest to the site of injury to attach to and crawl over the underlying dermal collagen network.²⁰ Cellular motility involves assembly and contraction of intracellular actinomyosin filaments. As with any injury, there is a lag time preceding cellular motion associated with the time required to loosen hemidesmosome attachments and the formation of new actin filament networks to enable motility.²¹

Of the 105,000 confocal images that were analyzed to determine the state of healing for each lesion, Probit analysis

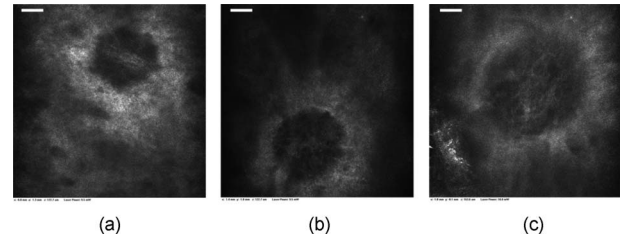


Fig. 11 Confocal view of coagulated dermis ~40-h post-treatment showing early signs of a collagen remodeling process, evidenced by viable structural details inside previously void coagulated dermal collagen (a) 30, (b) 40, and (c) 70 mJ. Scales indicate 50 μ m.

showed a distinct correlation between treatment energy and epidermal healing time. MTZ diameter increases with treatment energy, and based on our confocal observations, we estimated at least a 3 to 6-h time delay before epidermal changes due to keratinocyte migration to the site of injury became apparent. The larger the cross sectional area of the MTZ, the longer it takes for the tissue to fully re-epithelialize (Fig. 5).

Although we noted that in most cases basal keratinocytes initiated migration along the DEJ during wound healing, we also observed on occasion that suprabasal keratinocytes migration patterns preceded that of their basal counterparts. This has already been speculated about, and some evidence was presented in the literature.²² Our histology at 7- and 16-h post-treatment demonstrated evidence supporting both scenarios of epithelial keratinocyte migration and re-epithelialization (Figs. 8–10). As expected, HE staining of samples at time points immediate and 7-h post-treatment shows epidermal as well as dermal tissue coagulation. We also used LDH-stained histological tissue sections to distinguish between viable and nonviable tissue (Figs. 9 and 10). LDH staining proved particularly useful at identifying migrating basal or suprabasal keratinocytes within the area of prior fractional tissue necrosis.

Substantial evidence is provided by Figs. 7–10, which shows that DEJ and epidermal disruption is repaired and re-epithelialized by the keratinocytes that begin their migration from the perimeter of the coagulated tissue. In this manner, epidermal disruption visible with confocal microscopy gets filled in and becomes compacted as newly forming keratinocytes slowly occupy the same space, displacing the necrosed material toward the skin surface. Thus the boundaries of epidermal disruption get pushed closer together and are filled with viable cells.

Such detailed study and analysis of epidermal wound healing post fractional photothermolysis provides a solid foundation for understanding the implications and relevance of treatment spot size during fractional laser treatment procedures. With a finite cellular migration velocity and cell division, the time required to repair epidermal lesions tends to increase with the cross sectional dimension, and this trend is well documented in Fig. 5. The data illustrate the ability of the epidermis to completely re-epithelialize within less than 24 h up to 60-mJ treatment energy. The standard deviation, i.e., upper and lower time limit at 70 mJ, is slightly larger due to difficulties in continuous monitoring beyond 24 h at 1-h time

increments. Regardless, even at 70 mJ, 84% of all lesions have completely healed by 28-h post-treatment.

Combined with a better understanding of the re-epithelialization mechanism and keratinocyte migration pattern, one may expect significantly longer healing times with lesion or MTZ sizes that far exceed 500 μm . Large fractional spot size treatments also have a tendency to produce large MENDs, which tend to be more visible macroscopically in comparison to smaller spot sizes. Unnecessarily prolonged epidermal healing times may extend the duration of epidermal discomfort and erythema and, combined with clearly visible MENDs, cause greater patient dissatisfaction.

5 Conclusion

In conclusion, *in vivo* wound healing analysis using confocal imaging reveals that if 24-h epidermal re-epithelialization is desired, an optical size of less than 500 μm is required. Wound sizes greater than 500 μm lead to progressively slower re-epithelialization, thereby mitigating the benefits of fractional treatment. When the DE junction remains disrupted, there is a potential for pigment drop-out, which can clinically appear as postinflammatory hypopigmentation. We recommend treatment spot sizes of less than 500 μm to best capitalize on the benefits of nonablative fractional resurfacing technologies at 1550 nm.

Acknowledgment

The authors thank Jackson Fan for his participation in the study.

References

1. D. Manstein, G. S. Herron, R. K. Sink, H. Tanner, and R. R. Anderson, "Fractional photothermolysis: a new concept for cutaneous remodeling using microscopic patterns of thermal injury," *Lasers Surg. Med.* **34**, 426–438 (2004).
2. S. R. Cohen, C. Henssler, K. Horton, K. W. Broder, and P. A. Moise-Broder, "Clinical experience with the Fraxel SR laser: 202 treatments in 59 consecutive patients," *Plast. Reconstr. Surg.* **121**(5), 297–304 (2008).
3. R. J. Chiu and R. W. Kridel, "Fractionated photothermolysis: the Fraxel 1550-nm glass fiber laser treatment," *Facial Plast. Surg. Clin. North Am.* **15**(2), 229–237 (2008).
4. S. S. Collawn, "Fraxel skin resurfacing," *Ann. Plast. Surg.* **58**(3), 237–240 (2007).
5. M. H. Jih and A. Kimyai-Asadi, "Fractional photothermolysis: a review and update," *Semin Cutan Med. Surg.* **27**(1), 63–71 (2008).
6. B. Hantash, V. Bedi, S. Sudireddi, S. K. Struck, S. G. Herron, and K. F. Chan, "Laser-induced transepidermal elimination of dermal content by fractional photothermolysis," *J. Biomed. Opt.* **11**(4), 041115 (2006).
7. H. J. Laubach, Z. Tannous, R. R. Anderson, and D. Manstein, "Skin responses to fractional photothermolysis," *Lasers Surg. Med.* **38**(2), 142–149 (2006).
8. V. P. Bedi, K. F. Chan, R. K. Sink, B. M. Hantash, G. S. Herron, Z. Rahman, S. K. Struck, and C. B. Zachary, "The effects of pulse energy variations on the dimensions of microscopic thermal treatment zones in nonablative fractional resurfacing," *Lasers Surg. Med.* **39**(2), 145–155 (2007).
9. D. J. Finney, *Probit Analysis*, 3rd ed., Cambridge University Press, Cambridge, UK (1971).
10. B. Lund, Probit Fit, version 1.0.2, United States Army Medical Research Detachment Walter Reed Army Institute of Research Brooks City-Base, Texas (2004).
11. S. Thongsima, D. Zurakowski, and D. Manstein, "Histological comparison of two different fractional photothermolysis devices emitting at 1550 nm (abstr.)," *Lasers Surg. Med.* **40**(S20), 26 (1997).
12. N. J. Vardaxis, T. A. Brans, M. E. Boon, R. W. Kreis, and L. M. Marres, "Confocal laser scanning microscopy of porcine skin: implications for human wound healing studies," *J. Anat.* **190**, 601–611 (1997).
13. S. Gonzalez, K. Swindells, M. Rajadhyaksha, and A. Torres, "Changing paradigms in dermatology: confocal microscopy in clinical and surgical dermatology," *Clin. Dermatol.* **21**(5), 359–369 (2003).
14. M. Rajadhyaksha, S. Gonzalez, J. M. Zavislan, R. R. Anderson, and R. H. Webb, "In vivo confocal scanning laser microscopy of human skin II: advances in instrumentation and comparison with histology," *J. Invest. Dermatol.* **113**(3), 293–303 (1999).
15. P. Martin et al., "Wound healing—aiming for perfect skin regeneration," *Science* **276**, 75–81 (1997).
16. J. T. Beckman, M. A. Mackanos, C. Crooke, T. Takahashi, C. O'Connell-Rodwell, C. H. Contag, and E. D. Jansen, "Assessment of cellular response to thermal laser injury through bioluminescence imaging of heat shock protein 70," *Photochem. Photobiol.* **79**(1), 76–85 (2004).
17. C. F. Cheng, J. Fan, M. Fedesco, S. Guan, Y. Li, B. Bandyopadhyay, A. M. Bright, D. Yerushalmi, M. Liang, M. Chen, Y. P. Han, D. T. Woodley, and W. Li, "Transforming growth factor alpha (TGF α)-stimulated secretion of HSP90 α : using the receptor LRP-1/CD91 to promote human skin cell migration against a TGF β -rich environment during wound healing," *Mol. Cell. Biol.* **28**(10), 3344–3358 (2008).
18. A. F. Laplante, V. Moulin, F. A. Auger, J. Landry, H. Li, G. Morrow, R. M. Tanguay, and L. Germain, "Expression of heat shock proteins in mouse skin during wound healing," *J. Histochem. Cytochem.* **46**(11), 1291–1301 (1998).
19. J. M. Breuss, J. Gallo, H. M. DeLisser, I. V. Klimanskaya, H. G. Folkesson, J. F. Pittet et al., "Expression of the beta 6 integrin subunit in development, neoplasia and tissue repair suggests a role in epithelial remodeling," *J. Cell. Sci.* **108**(6), 2241–2251 (1995).
20. A. Cavani, G. Zambruno, A. Marconi, V. Manca, M. Marchetti, and A. Giannetti, "Distinctive integrin expression in the newly forming epidermis during wound healing in humans," *J. Invest. Dermatol.* **101**, 600–604 (1993).
21. F. Grinnell, "Wound repair, keratinocyte activation and integrin modulation," *J. Cell. Sci.* **101**, 1–5 (1992).
22. J. A. Garlick and L. B. Taichman, "Fate of human keratinocytes during reepithelialization in an organotypic culture model," *Lab. Invest.* **70**(6), 916–924 (1994).